

See discussions, stats, and author profiles for this publication at: <https://www.researchgate.net/publication/259209974>

Lithium Ion Battery Performance of Silicon Nanowires with Carbon Skin

ARTICLE *in* ACS NANO · DECEMBER 2013

Impact Factor: 12.88 · DOI: 10.1021/nn405710w · Source: PubMed

CITATIONS

51

READS

22

6 AUTHORS, INCLUDING:



Xiaotang Lu

University of Texas at Austin

15 PUBLICATIONS 392 CITATIONS

SEE PROFILE

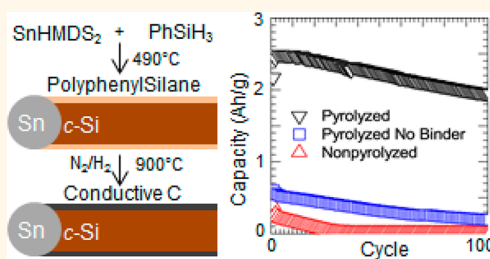
Lithium Ion Battery Performance of Silicon Nanowires with Carbon Skin

Timothy D. Bogart,[†] Daichi Oka,[‡] Xiaotang Lu,[†] Meng Gu,[§] Chongmin Wang,[§] and Brian A. Korgel^{†,*}

[†]Department of Chemical Engineering, Texas Materials Institute, Center for Nano- and Molecular Science and Technology, The University of Texas at Austin, Austin, Texas 78712-1062, United States, [‡]Department of Chemistry, School of Science, The University of Tokyo, 7-3-1 Hongo, Bunkyo, Tokyo 113-0033 Japan, and

[§]Environmental Molecular Sciences Laboratory, Pacific Northwestern National Laboratory, Richland, Washington 99354, United States

ABSTRACT Silicon (Si) nanomaterials have emerged as a leading candidate for next generation lithium-ion battery anodes. However, the low electrical conductivity of Si requires the use of conductive additives in the anode film. Here we report a solution-based synthesis of Si nanowires with a conductive carbon skin. Without any conductive additive, the Si nanowire electrodes exhibited capacities of over 2000 mA h g⁻¹ for 100 cycles when cycled at C/10 and over 1200 mA h g⁻¹ when cycled more rapidly at 1C against Li metal. *In situ* transmission electron microscopy (TEM) observation reveals that the carbon skin performs dual roles: it speeds lithiation of the Si nanowires significantly, while also constraining the final volume expansion. The present work sheds light on ways to optimize lithium battery performance by smartly tailoring the nanostructure of composition of materials based on silicon and carbon.



KEYWORDS: silicon · tin · nanowires · anode · carbon coating · lithium-ion battery · *in situ* TEM

As the power demands of mobile technologies continue to increase, lithium (Li)-ion batteries are needed with greater power and energy density.¹ Silicon (Si) anodes offer an alternative to commercial graphite with much greater gravimetric and volumetric Li storage capacity (Li₁₅Si₄, 3579 mA h g⁻¹, 8334 A h L⁻¹ vs LiC₆, 372 mA h g⁻¹, 804 A h L⁻¹).^{2,3} Si anodes could improve the charge capacity of existing Li-ion batteries by more than 30% and could enable an order of magnitude improvement if paired with a next generation cathode like sulfur.^{4,5} The main limitations of Si in Li-ion batteries are the massive volume changes that occur during cycling and poor electrical conductivity.⁶ Nanoscale Si can mostly tolerate the volume changes,^{7–10} and Si nanowires are particularly compelling anode materials because they provide short Li diffusion paths due to their narrow diameter (<100 nm) combined with long (>1 μm) continuous paths for electron transport down their length.^{11–25}

Silicon nanowires can be produced by vapor–liquid–solid (VLS) growth on metal substrates to obtain intimate electrical contact with the current collector in the battery, but only with very low mass loadings of less than about 200 μg/cm² that cannot provide

enough current for most needs.^{26–29} Mass loadings greater than 1 mg/cm², which are more appropriate for most applications, require relatively thick electrode layers. These are usually obtained by doctor-blading slurries with significant amounts of Si. Because of the synthetic limitations of VLS, many groups turn to commercially available Si powder for slurry-based anodes, but sufficient amounts of Si nanowires can be obtained using solution-based syntheses, like solution–liquid–solid (SLS) or supercritical fluid–liquid–solid (SFLS) methods.^{6,18,25,30–33}

To achieve reasonable battery performance in the relatively thick slurry-based Si anodes, conductive carbon particles must be added (usually ~10% by weight) to provide sufficient electrical conductivity through the layer. This lowers the capacity of the anode, but more importantly, the carbon particles can segregate in the electrode layer during processing or as a result of mechanical stresses during cycling, leading to unreliable performance.³⁴ Better electrical contact can be achieved by encapsulating the Si nanomaterials in carbon.^{23,35–43} Carbon encapsulation improves adhesion to the Si material, thus improving electrode stability and electrical conductivity through the film, as well as providing additional mechanical

* Address correspondence to korgel@che.utexas.edu.

Received for review November 3, 2013 and accepted December 6, 2013.

Published online December 06, 2013
10.1021/nn405710w

© 2013 American Chemical Society

support against the stresses that occur during volume expansion and contraction.^{35–37} The carbon coating can also create a protective barrier that prevents unwanted side reactions between the Si surface and the electrolyte to form a robust solid electrolyte interphase (SEI) layer.^{42–45}

Here, we report the performance of tin-seeded Si nanowires with conformal carbon coatings in lithium ion batteries. The nanowires are produced by SFLS growth using phenylsilane and Sn(HMDS)₂ as reactants. Straight and crystalline Si nanowires are produced, with a polyphenylsilane shell that is then pyrolyzed into a conformal conductive carbon coating. The *in situ* seeding approach in which Sn(HMDS)₂ decomposes to Sn seed particles in the reactor saves a processing step since metal seed particles do not need to be made prior to the nanowire growth reaction.^{25,46–48} Sn is also a very suitable seed metal for lithium ion battery applications as it is much lighter than commonly used gold (Au) and actively participates in the lithiation reactions.^{25,49} Nanowire battery performance was tested in half-cells and by *in situ* TEM imaging of individual nanowires undergoing lithiation. The *in situ* TEM experiments showed that the carbon coating increases the rate of Si lithiation by nearly an order of magnitude compared to bare Si nanowires and restricts the nanowire volume expansion during lithiation.

RESULTS AND DISCUSSION

Si Nanowires. Figure 1 shows SEM and TEM images and XRD of the Si nanowire product obtained from reactions carried out with various Si:Sn ratios, while Figure 2 illustrates the reaction pathway that occurs during nanowire growth. MPS decomposes by phenyl redistribution to silane (SiH₄) and higher order phenylsilanes.⁵⁰ Sn(HMDS)₂ decomposes to Sn, which forms a eutectic with Si at relatively low temperature (232 °C) and seeds crystalline nanowire growth from Si generated from silane decomposition. The higher order phenylsilane byproduct polymerizes at the nanowire surface to form a polyphenylsilane shell. As shown in Figure 1, the morphology of the nanowire product is highly sensitive to the Si:Sn ratio. At Si:Sn ratios above 32 (Figure 1e–h), the nanowires are heavily kinked and covered in a thick polyphenylsilane shell. The nanowires made with Si:Sn ratios below 22 (Figure 1a–d) are markedly straighter with significantly decreased shell thickness. X-ray diffraction (XRD), Figure 1i, shows that the nanowires are diamond cubic Si with Sn present in the nanowires synthesized at higher Sn loadings.

Compared to MPS reactions using Au nanocrystals to seed Si nanowire growth, proportionally much more Sn is needed to obtain straight and crystalline nanowires. For example, the typical Si:Au ratio used for SFLS growth of Si nanowires with MPS is 666,⁵¹ whereas the

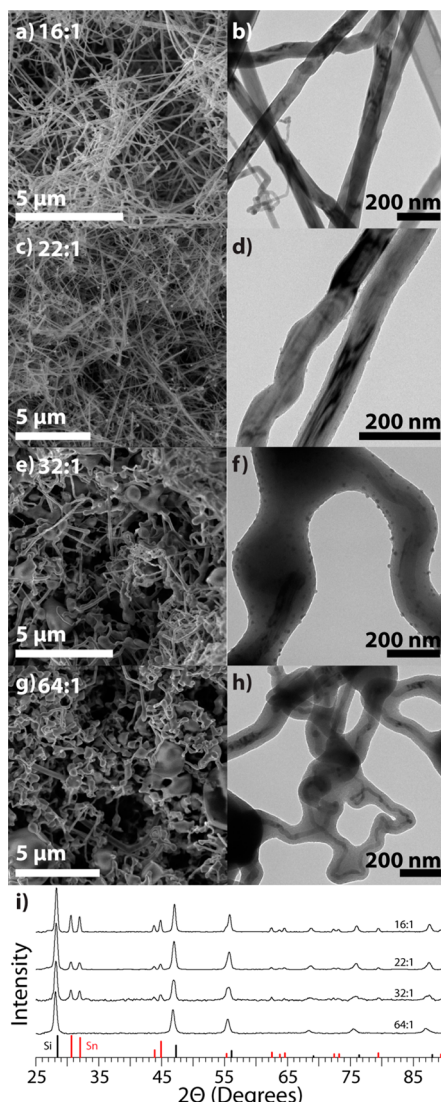


Figure 1. Si nanowires grown from different ratios of MPS and Sn(HMDS)₂. The SEM and TEM images show that the nanowires are made increasingly straight with less polyphenylsilane shell material by decreasing the Si:Sn molar ratio: (a and b) 16, (c and d) 22, (e and f) 32, and (g and h) 64. (i) XRD of the reaction products is compared to Si and Sn reference patterns (JCPDS reference patterns: Si (black) 00–027–1402, tetragonal β-Sn (red) 00–004–0673).

best Sn-seeded Si nanowires are made with Si:Sn ratios of between 16 and 22. It appears that more Sn is required in the reactions because a large amount of Sn incorporates into the nanowires during growth, which does not happen with Au.^{46,52} Figure 3 shows TEM and HAADF-STEM images, and EDS compositional maps of Si and Sn, of nanowires synthesized with a Si:Sn ratio of 22 before and after shell pyrolysis. The shell is clearly visible before (Figure 3a) and after (Figure 3b) pyrolysis, and carbon shell retains the thickness uniformity of the polyphenylsilane shell. EDS line scans (Figures 3c–f) show significant quantities of Sn in the nanowires. There is about 2.15 atom % Sn, which is well above the solid solubility of 0.018 atom % at the growth temperature of 490 °C.⁵³ The bright spots in

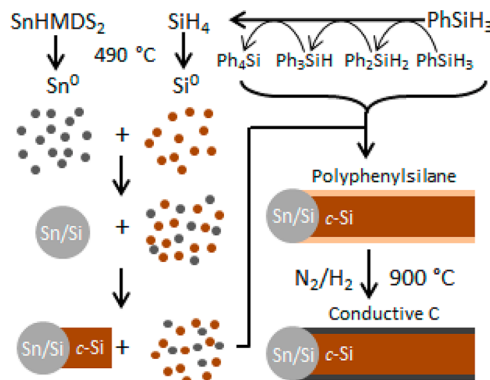


Figure 2. Synthesis of Si nanowires with conformal carbon coatings. $\text{Sn}(\text{HMDS})_2$ decomposes to Sn particles that seed Si nanowire growth by the SFLS mechanism. Monophenylsilane decomposes via phenyl redistribution to produce SiH_4 , which decomposes into atomic Si, and higher order phenylsilane byproducts that lead to the polyphenylsilane shell.⁵⁰ After nanowire synthesis, the polyphenylsilane shell is pyrolyzed to conductive carbon by heating to 900 °C under forming gas.

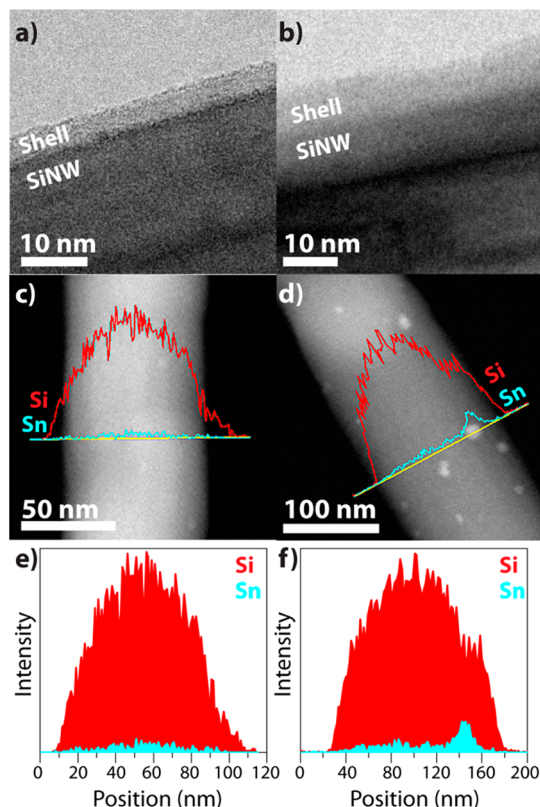


Figure 3. HRTEM, HAADF-STEM, and EDS line scans of the Sn-seeded Si nanowires grown using a Si:Sn molar ratio of 22 (a, c, and e) before and (b, d, and f) after pyrolysis of the polyphenylsilane shell by heating for 1 h at 900 °C under forming gas. The bright spots correspond to pockets of Sn that reside within the core of the nanowire, which remain after pyrolysis.

the HAADF-STEM image in the Si nanowire correspond to pockets of Sn encapsulated in the nanowire.

Electrochemical Testing. Si nanowires synthesized with a Si:Sn mole ratio of 22 were tested in batteries vs Li

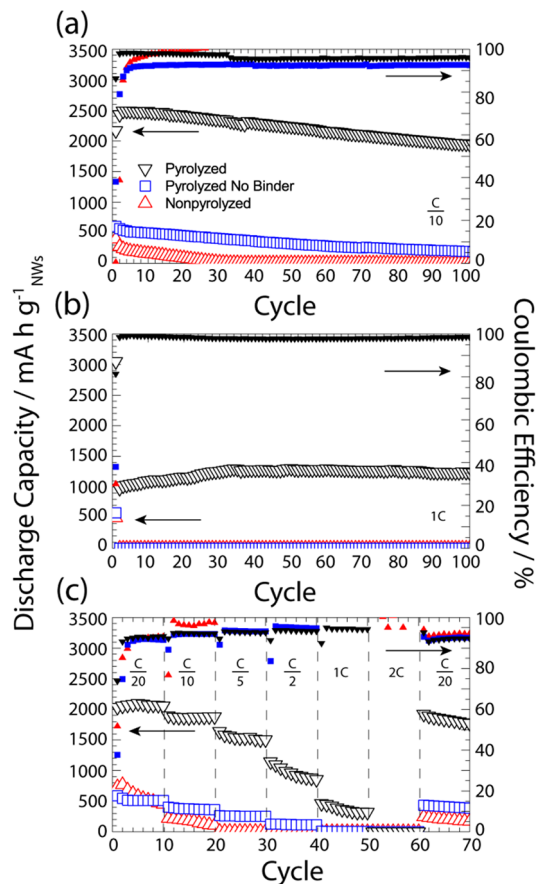


Figure 4. Capacity of anodes made from Si nanowires and PAA before pyrolysis (red up-triangles), after pyrolysis (black down-triangles), and after pyrolysis but without using any PAA binder (blue squares). Anodes were fabricated without additional conductive carbon. Batteries were cycled at (a) C/10 for 100 cycles, (b) 1C for 100 cycles, and (c) various rates between C/20 and 2C for 10 cycles each vs Li metal.

metal. These nanowires were relatively straight, crystalline and had a thin polyphenylsilane shell that could be pyrolyzed to carbon. Figure 4 shows battery data for Si anodes made by combining the nanowires with PAA binder. Capacities are reported based on the weight of the nanowires including the carbon shell. The pyrolyzed nanowires exhibited high capacities, over 2000 mA h g^{-1} , with nearly 96% Coulombic efficiency when cycled at the slow rate of C/10 for 100 cycles. An increased cycle rate led to decreased capacity, but the nanowires still showed a stable capacity of about 1300 mA h g^{-1} with greater than 98% Coulombic efficiency when cycled at 1C. The battery capacity dropped essentially to zero at the much faster cycle rate of 2C. Nanowires that were not pyrolyzed exhibited almost no capacity, with an initial capacity of about 300 mA h g^{-1} that faded to zero after about 20 cycles at C/10. Pyrolyzed nanowires tested without PAA binder also exhibited very limited capacity, of $<500 \text{ mA h g}^{-1}$ when cycled at C/10, and no measurable capacity when cycled faster than C/2. Fabrication of Si nanowire anodes without binder was also quite difficult as the

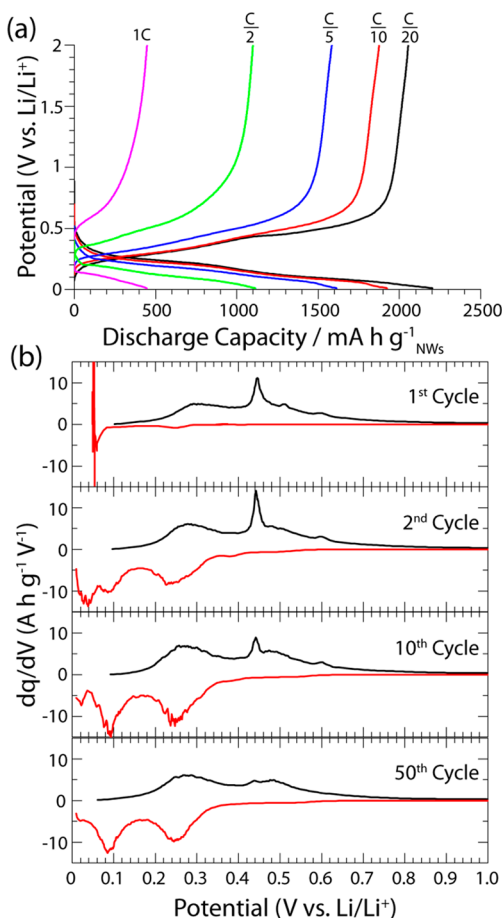


Figure 5. (a) Voltage–capacity curves for pyrolyzed Si nanowires cycled at various rates from C/20 to 1C. Profiles correspond to the 2nd cycle for each of the rates tested in Figure 4c. (b) Differential capacity plots for the 1st, 2nd, 10th, and 50th cycle of pyrolyzed Si nanowires cycled at C/10.

nanowires were poorly adhered to the Cu foil and easily flaked off the substrate.

The voltage profiles of the pyrolyzed Si nanowire with PAA anodes exhibited the typical characteristics of Si undergoing relatively stable lithiation and delithiation.^{12,15–18,20,22} Figure 5a shows the voltage profiles of the electrodes cycled at various rates and Figure 5b shows the corresponding differential capacity plots for the cycle rate of C/10. The first cycle differential capacity plot shows one peak for the lithiation at ~60 mV corresponding to the lithiation of c-Si and three main delithiation peaks; the sharp peak at ~450 mV corresponds to the delithiation of c-Li_xSi while the two broad peaks at ~300 and ~500 mV correspond to the delithiation of a-Li_xSi.^{3,14,25,38} There is also a small peak at ~400 mV in the lithiation and ~600 mV in the delithiation indicative of Sn.^{54–56} During the second cycle, additional lithiation peaks emerge at ~250 and ~100 mV corresponding to the lithiation of a-Si. This is to be expected as bare Si does not return to its crystalline state after the first cycle but rather becomes amorphous.⁵⁷ Throughout cycling, the crystalline lithiation and delithiation peaks decrease in

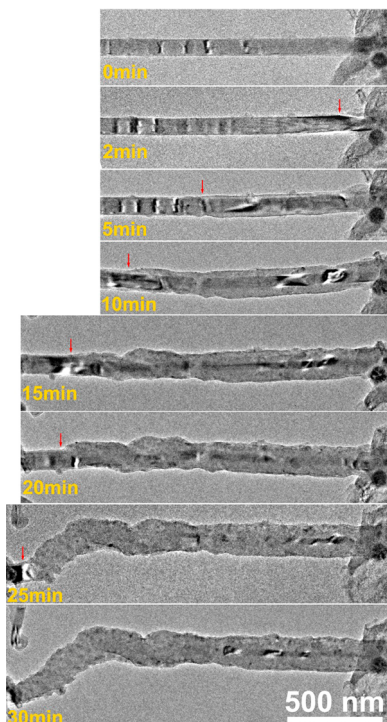


Figure 6. Time sequence of *in situ* lithiation of the pyrolyzed Si nanowires. Red arrow indicates the lithiation front propagating along the nanowire (video provided in Supporting Information).

intensity while the amorphous peaks grow stronger. This indicates that the carbon coating initially prevents the wire from fully converting to a-Li_xSi and maintaining regions with crystalline structure, but eventually breaks down through repeated cycling.

In Situ TEM Imaging of Pyrolyzed Si Nanowires Undergoing Lithiation. Coin cell battery tests provide a macroscopic, averaged measure of nanowire performance as they undergo lithiation and delithiation. To directly observe the morphology changes of individual Si nanowires with pyrolyzed carbon shells, *in situ* TEM experiments were performed. Figure 6 shows a sequence of TEM images of an Si nanowire with a pyrolyzed carbon shell undergoing lithiation (video supplied as Supporting Information). The nanowire is placed into contact with Li₂O-coated Li metal and a –3 V bias is applied to drive the lithiation. The lithiation begins at the point of contact between the nanowire and the Li₂O surface and travels quickly along the surface of the nanowire converting the c-Si to a-Li_xSi. During the first 10 min of lithiation, the majority of lithium diffusion occurs axially down the surface of the nanowire, traveling at a rate of almost 200 nm min⁻¹, which is approximately 50% faster than previously reported for bare Si nanowires.⁵⁸

Lithiation into the core of the nanowire does eventually take place and comes to completion after 30 min. The lithiated nanowire exhibits two distinctly different morphologies. The left side of the nanowire has begun to curl, whereas the right side of the nanowire remains

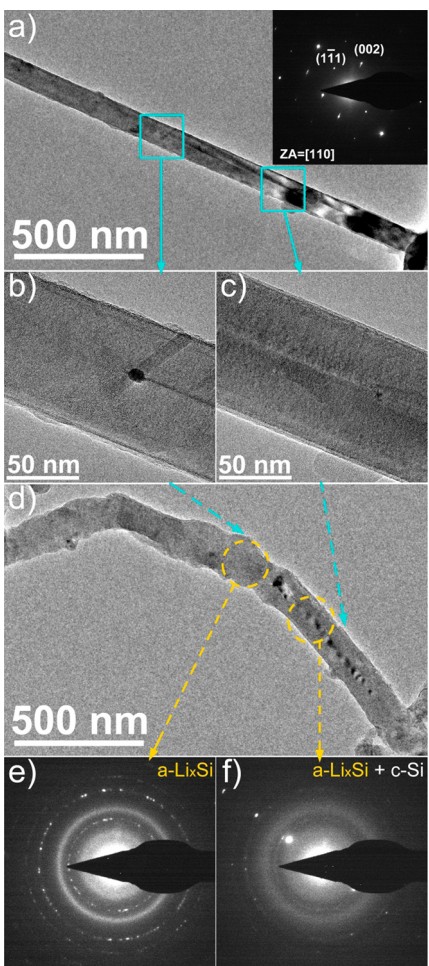


Figure 7. (a–c) HRTEM of a Si nanowire prior to *in situ* lithiation highlighting areas of the nanowire where the shell is (b) partially and (c) completely coating the nanowire surface. (d) HRTEM of the Si nanowire after *in situ* lithiation with selected area electron diffraction patterns of the (e) partially coated and (f) uniformly coated sections of the nanowire. In the partially coated section, the rings in the SAED show that the nanowire is composed of amorphous lithiated silicon with some spots indicative of Li oxide due to reaction with the native oxide found on the uncovered regions of the nanowire. In the uniformly coated section, the spot pattern and the amorphous rings indicate a crystalline Si core remains after lithiation and no pattern is visible for Li oxide.

relatively straight. The left side of the nanowire has fully converted to an amorphous lithiated Si phase, while the right side of the nanowires retains a thin crystalline or partially lithiated region. Extending the lithiation time had no effect on the morphology of this region of the nanowire. Figure 7 shows HRTEM and selected area electron diffraction (SAED) taken from each region of the nanowire. The HRTEM images revealed that the right side of the nanowire has a complete and uniform carbon coating (Figure 7c), while the carbon coating on the left section of the nanowire is nonuniform and incomplete (Figure 7b). The complete and uniform carbon shell prevents the Si nanowire from expanding enough to fully lithiate.⁵⁹ The SAED pattern taken from the right-hand side of the

nanowire (Figure 7f) shows both patterns corresponding to both *c*-Si and *a*-Li_xSi, indicating that the core has not been fully lithiated. The partial nonuniform carbon coating, however, gives way to the stress created by the expanding Si nanowire, and there is no sign of remaining *c*-Si in the SAED pattern obtained from the left region of the nanowire in Figure 7e. This kind of self-limiting lithiation has not been previously observed in *in situ* TEM experiments of carbon-coated Si nanowires; however, previous experiments of carbon-coated Si nanowires utilized an ionic liquid electrolyte that may have modified the carbon coating, possibly by creating pores and alleviating the stress.⁵⁸ Based on the shift from crystalline peaks to amorphous peaks in the differential capacity plots, it is likely that after repeated cycling the uniform coating begins to crack, relieving the stress and allowing the core to fully lithiate and become amorphous. The radial rate of lithiation, as measured by the change in *c*-Si core thickness over time, is also affected by the uniformity of the coating with the average velocity being 62 nm h⁻¹ when the nanowire is completely coated and 400 nm h⁻¹ when partially coated. It is worth noting that both of these rates are faster than the previously reported rate of 35 nm h⁻¹ for bare *c*-Si nanowires.⁵⁹

CONCLUSIONS

Sn(HMDS)₂ was used for *in situ* Sn seeding of crystalline Si nanowires with a polyphenylsilane shell via SFLS growth. The shell was pyrolyzed to a conductive carbon coating that eliminated the need for conductive additives in the electrodes made using the nanowires. HRTEM and STEM with EDS compositional mapping also showed that high amounts of Sn were present in the nanowires at greater than 2 atom %. *In situ* TEM measurements showed that the rate of lithiation in these nanowires was significantly faster than in typical Si nanowires by nearly an order of magnitude. Lithium ion battery electrodes made with Si nanowires coated by pyrolyzed carbon shells exhibited high capacities of over 2000 mA h g⁻¹ for 100 cycles when cycled slowly at C/10 and over 1200 mA h g⁻¹ when cycled quickly at 1C. Uniform and complete carbon coatings were also found to prevent complete nanowire expansion needed for full lithiation of the nanowire. On the basis of the battery cycling tests, however, it appears that the carbon shells probably begin to fail after many cycles, leading to full lithiation and amorphization of the nanowires.

These battery and TEM results show that coatings on Si nanowires can have a very significant impact on the lithiation/delithiation behavior of the material. A couple of effects were observed. The first was the speeding up of the lithiation rate in the nanowires, by nearly an order of magnitude. The second was the mechanical stress applied by the core that prevented full lithiation of the Si material. It remains to be seen now what the

optimum role of such conformal shells may be for Si (and probably Ge too) anodes in lithium ion batteries. The *in situ* TEM experiments presented here clearly

show that such shells can stabilize the nanowire morphology, but also prevents full lithiation and can eventually fail over the course of many cycles.

EXPERIMENTAL DETAILS

Materials. All reagents and solvents were used as received. Chloroform (99.9%), ethanol (EtOH, 99.9%), toluene (anhydrous, 99.8%), bis(bis(trimethylsilyl)amino)tin ($\text{Sn}(\text{HMDS})_2$, 99.8%), poly(acrylic acid) (PAA, $M_v \sim 450\,000$), 1-methyl-2-pyrrolidinone (NMP, anhydrous 99.5%), lithium hexafluorophosphate (LiPF_6 , ≥99.99%), ethylene carbonate (EC, 99%), and diethyl carbonate (DEC, ≥99%, anhydrous) were purchased from Sigma-Aldrich. Monophenylsilane (MPS) was purchased from Gelest, Inc. Li metal foil (1.5 mm 99.9%) was purchased from Alfa Aesar and fluoroethylene carbonate (FEC, >98%) was purchased from TCI America. Celgard 2400 membranes (25 μm) were supplied by Celgard and conductive carbon super C65 was provided by TIMCAL. Coin cells (2032 stainless steel) and copper (Cu) foil (9 μm thick) were purchased from MTI Corporation.

Silicon Nanowire Synthesis and Carbon Shell Formation. Si nanowires were prepared by supercritical fluid–liquid–solid (SFLS) growth using MPS and Sn seeds generated *in situ* in the reactor from $\text{Sn}(\text{HMDS})_2$.^{25,31,46,51} A titanium reactor is loaded with toluene and heated and pressurized to 490 °C and 10.3 MPa. A reactant solution with a Si:Sn mole ratio of 64 is prepared in an argon-filled glovebox (<0.1 ppm O₂) by combining 500 μL of MPS and 24 μL of $\text{Sn}(\text{HMDS})_2$ in 30 mL of anhydrous toluene and then loaded into an injection cylinder. Reactions were also carried out using Si:Sn mole ratios of 32, 22, and 16 by increasing the amount of $\text{Sn}(\text{HMDS})_2$ to 48, 72, and 96 μL , respectively. Reactant solutions are injected at a rate of 0.5 mL/min for 40 min using a micrometer valve to maintain constant pressure in the reactor. Immediately after finishing with the reactant injection, the reactor is sealed and removed from the heating block to cool overnight to room temperature. The crude reaction product is extracted from the reactor with toluene. The reaction product is precipitated by centrifugation at 8000 rpm for 5 min and the supernatant is discarded. The nanowires are washed three times by repeated dispersion in a 2:1:1 chloroform:toluene:ethanol mixture, centrifugation, and decanting of the supernatant. Multiple batches of purified nanowires, approximately 25 mg each, are then combined and dried on a rotary evaporator. Approximately 100 mg of the combined nanowire material is then loaded into a quartz tube furnace and purged for 30 min with forming gas (93% N₂/7% H₂). The material is then heated at 900 °C for 1 h under constant forming gas flow.

Characterization Methods. Scanning electron microscopy (SEM) images were acquired with a Zeiss Supra 40 SEM with an in-lens arrangement at 2 kV and 5 mm working distance. For imaging, the nanowires were deposited on polished silicon wafers. Transmission electron microscopy (TEM) images were digitally acquired using a field emission JEOL 2010F TEM operated at 200 kV with nanowire samples deposited on 200 mesh lacey-carbon copper TEM grids (Electron Microscopy Sciences). Energy-dispersive X-ray spectroscopy (EDS) line scans were performed with an Oxford Inca EDS detector on the JEOL 2010F TEM operated in high angle annular dark field (HAADF) scanning transmission electron microscopy (STEM) mode. X-ray diffraction (XRD) was performed using a Rigaku R-Axis Spider Diffractometer and Image plate detector. Samples were prepared on a 0.5 mm nylon loop and scanned for 15 min at 1°/s sample rotation under Cu K α ($\lambda = 1.5418\text{ \AA}$) radiation at 40 kV and 40 mA.

Electrochemical Testing. Si nanowire slurries were prepared by combining 80 mg of Si nanowires with PAA (4:1 w/w Si:PAA) in 1.5 mL of NMP. The mixture was probe sonicated for 30 min. Slurries were doctor-bladed (200 μm gap) onto Cu foil and dried at 80 °C overnight under vacuum. Individual 11 mm diameter circular electrodes were hole-punched from the coated Cu foil. Typical mass loadings were 0.25–0.8 mg cm^{-2} . Electrodes tested without PAA binder were made using the same procedure. Coin cells (2032 stainless steel) were assembled in an

argon-filled glovebox (<0.1 ppm O₂) using Li foil as the counter electrode, 1.0 M LiPF₆ in 1:1 w/w EC:DEC with 5 wt % FEC as the electrolyte solution, and Celgard 2400 membranes as the separator. Coin cells were crimped and removed from the glovebox for testing with an Arbin BT-2143 test unit cycling between 2.0 and 0.01 V vs Li/Li⁺. Capacities are reported based on the total weight of the anode material. It was calculated from TEM images and the densities of Si and graphitic carbon that the carbonaceous shell accounts for approximately 10% of the weight of the nanowires and the PAA binder was assumed to be electrochemically inactive resulting in an overall anode capacity of $C = 2617\text{ mAh g}^{-1}$ for deriving cycle rates used in testing.

In Situ TEM Imaging of Si Nanowire Lithiation. *In situ* TEM imaging was performed using a Titan 80–300 scanning/transmission electron microscope (S/TEM) and a Nanofactory TEM holder. The nanobattery consisting of Si nanowires drop cast on a tungsten wire as the anode and lithium as the cathode was assembled in an Ar-filled glovebox. The TEM holder was then transferred from the glovebox to the microscope in a sealed Ziploc plastic bag. The TEM nanobattery was exposed to air briefly during loading into the microscope. Air exposure was less than 5 s, during which time a thin Li₂O layer forms on the Li metal surface that serves as a solid state electrolyte for the nanobattery. A –3 V bias was applied to lithiate the nanowires, and delithiation was carried out by applying a 3 V bias. The beam intensity was minimized using a beam current of ~1 mA cm^{-2} to avoid beam effects.

Conflict of Interest: The authors declare no competing financial interest.

Acknowledgment. This work was funded by the Robert A. Welch Foundation (grant no. F-1464) and as part of the program “Understanding Charge Separation and Transfer at Interfaces in Energy Materials (EFRC: CST),” an Energy Frontier Research Center funded by the U.S. Department of Energy Office of Science, Office of Basic Energy Sciences, under Award No. DE-SC0001091. *In situ* TEM imaging was performed in the William R. Wiley Environmental Molecular Sciences Laboratory (EMSL), a national scientific user facility sponsored by DOE’s Office of Biological and Environmental Research and located at PNNL. PNNL is operated by Battelle for the DOE under Contract DE-AC05-76RLO1830. T.D.B acknowledges financial support from the Department of Defense through the National Defense Science & Engineering Graduate Fellowship Program. D.O. acknowledges the National Nanotechnology Infrastructure Network for financial support *via* the NSF Grant No. ECCS-0335765, and the Nanotechnology Platform of the Ministry of Education, Culture, Sports, Science and Technology (MEXT), Japan. C.M.W. and M.G. acknowledge the support of the Chemical Imaging Initiative at Pacific Northwest National Laboratory (PNNL).

Supporting Information Available: Movie (c_Si_1stLithiation_compress) showing *in situ* TEM imaging of a carbon-coated Si nanowire undergoing electrochemical lithiation. This material is available free of charge *via* the Internet at <http://pubs.acs.org>.

REFERENCES AND NOTES

- Tarascon, J.-M.; Armand, M. Issues and Challenges Facing Rechargeable Lithium Batteries. *Nature* **2001**, *414*, 359–367.
- Obrovac, M. N.; Christensen, L. Structural Changes in Silicon Anodes During Lithium Insertion/Extraction. *Electrochim. Solid-State Lett.* **2004**, *7*, A93–A96.
- Li, J.; Dahn, J. R. An *In Situ* X-ray Diffraction Study of the Reaction of Li with Crystalline Si. *J. Electrochem. Soc.* **2007**, *154*, A156–A161.

4. Yang, Y.; McDowell, M. T.; Jackson, A.; Cha, J. J.; Hong, S. S.; Cui, Y. New Nanostructured Li₂S/Silicon Rechargeable Battery with High Specific Energy. *Nano Lett.* **2010**, *10*, 1486–1491.
5. Elazari, R.; Salitra, G.; Gershinsky, G.; Garsuch, A.; Panchenko, A.; Aurbach, D. Rechargeable Lithiated Silicon–Sulfur (SLS) Battery Prototypes. *Electrochim. Commun.* **2012**, *14*, 21–24.
6. Bogart, T. D.; Chockla, A. M.; Korgel, B. A. High Capacity Lithium Ion Battery Anodes of Silicon and Germanium. *Curr. Op. Chem. Eng.* **2013**, *2*, 286–293.
7. Boukamp, B. A.; Lesh, G. C.; Huggins, R. A. All-Solid Lithium Electrodes with Mixed-Conductor Matrix. *J. Electrochem. Soc.* **1981**, *128*, 725–729.
8. Beaulieu, L. Y.; Eberman, K. W.; Turner, R. L.; Krause, L. J.; Dahn, J. R. Colossal Reversible Volume Changes in Lithium Alloys. *Electrochim. Solid-State Lett.* **2001**, *4*, A137–A140.
9. Ryu, I.; Choi, J. W.; Cui, Y.; Nix, W. D. Size-Dependent Fracture of Si Nanowire Battery Anodes. *J. Mech. Phys. Solids* **2011**, *59*, 1717–1730.
10. Liu, X. H.; Zhong, L.; Huang, S.; Mao, S. X.; Zhu, T.; Huang, J. Y. Size-Dependent Fracture of Silicon Nanoparticles During Lithiation. *ACS Nano* **2012**, *6*, 1522–1531.
11. Huang, R.; Fan, X.; Shen, W.; Zhu, J. Carbon-Coated Silicon Nanowire Array Films for High-Performance Lithium-Ion Battery Anodes. *Appl. Phys. Lett.* **2009**, *95*, 133119–133119–3.
12. Cui, L.-F.; Yang, Y.; Hsu, C.-M.; Cui, Y. Carbon–Silicon Core–Shell Nanowires as High Capacity Electrode for Lithium Ion Batteries. *Nano Lett.* **2009**, *9*, 3370–3374.
13. Xu, W.; Flake, J. C. Composite Silicon Nanowire Anodes for Secondary Lithium-Ion Cells. *J. Electrochem. Soc.* **2010**, *157*, A41–A45.
14. Cui, L.-F.; Ruffo, R.; Chan, C. K.; Peng, H.; Cui, Y. Crystalline-Amorphous Core–Shell Silicon Nanowires for High Capacity and High Current Battery Electrodes. *Nano Lett.* **2009**, *9*, 491–495.
15. Hieu, N. S.; Lim, J. C.; Lee, J. K. Free-Standing Silicon Nanorods on Copper Foil as Anode for Lithium-Ion Batteries. *Microelectron. Eng.* **2012**, *89*, 138–140.
16. Chan, C. K.; Peng, H.; Liu, G.; McIlwraith, K.; Zhang, X. F.; Huggins, R. A.; Cui, Y. High-Performance Lithium Battery Anodes Using Silicon Nanowires. *Nat. Nanotechnol.* **2008**, *3*, 31–35.
17. Yao, Y.; Liu, N.; McDowell, M. T.; Pasta, M.; Cui, Y. Improving the Cycling Stability of Silicon Nanowire Anodes with Conducting Polymer Coatings. *Energy Environ. Sci.* **2012**, *5*, 7927–7930.
18. Chockla, A. M.; Bogart, T. D.; Hessel, C. M.; Klavetter, K. C.; Mullins, C. B.; Korgel, B. A. Influences of Gold, Binder and Electrolyte on Silicon Nanowire Performance in Li-ion Batteries. *J. Phys. Chem. C* **2012**, *116*, 18079–18086.
19. Du, N.; Zhang, H.; Fan, X.; Yu, J.; Yang, D. Large-Scale Synthesis of Silicon Arrays of Nanowire on Titanium Substrate as High-performance Anode of Li-ion Batteries. *J. Alloys Compd.* **2012**, *526*, 53–58.
20. Chakrapani, V.; Rusli, F.; Filler, M. A.; Kohl, P. A. Silicon Nanowire Anode: Improved Battery Life with Capacity-Limited Cycling. *J. Power Sources* **2012**, *205*, 433–438.
21. Huang, R.; Zhu, J. Silicon Nanowire Array Films as Advanced Anode Materials for Lithium-Ion Batteries. *Mater. Chem. Phys.* **2010**, *121*, 519–522.
22. Chockla, A. M.; Harris, J. T.; Akhavan, V. A.; Bogart, T. D.; Holmberg, V. C.; Steinhagen, C.; Mullins, C. B.; Stevenson, K. J.; Korgel, B. A. Silicon Nanowire Fabric as a Lithium Ion Battery Electrode Material. *J. Am. Chem. Soc.* **2011**, *133*, 20914–20921.
23. Chan, C. K.; Patel, R. N.; O'Connell, M. J.; Korgel, B. A.; Cui, Y. Solution-Grown Silicon Nanowires for Lithium-Ion Battery Anodes. *ACS Nano* **2010**, *4*, 1443–1450.
24. Xu, W.; Vegunta, S. S. S.; Flake, J. C. Surface-Modified Silicon Nanowire Anodes for Lithium-Ion Batteries. *J. Power Sources* **2011**, *196*, 8583–8589.
25. Chockla, A. M.; Klavetter, K. C.; Mullins, C. B.; Korgel, B. A. Tin-Seeded Silicon Nanowires for High Capacity Li-ion Batteries. *Chem. Mater.* **2012**, *24*, 3738–3745.
26. Laik, B.; Eude, L.; Pereira-Ramos, J.-P.; Cojocaru, C. S.; Pribat, D.; Rouvière, E. Silicon Nanowires as Negative Electrode for Lithium-Ion Microbatteries. *Electrochim. Acta* **2008**, *53*, 5528–5532.
27. Ruffo, R.; Hong, S. S.; Chan, C. K.; Huggins, R. A.; Cui, Y. Impedance Analysis of Silicon Nanowire Lithium Ion Battery Anodes. *J. Phys. Chem. C* **2009**, *113*, 11390–11398.
28. Chakrapani, V.; Rusli, F.; Filler, M. A.; Kohl, P. A. Quaternary Ammonium Ionic Liquid Electrolyte for a Silicon Nanowire-Based Lithium Ion Battery. *J. Phys. Chem. C* **2011**, *115*, 22048–22053.
29. Yuan, F.-W.; Yang, H.-J.; Tuan, H.-Y. Seeded Silicon Nanowire Growth Catalyzed by Commercially Available Bulk Metals: Broad Selection of Metal Catalysts, Superior Field Emission Performance, and Versatile Nanowire/Metal Architectures. *J. Mater. Chem.* **2011**, *21*, 13793–13800.
30. Hanrath, T.; Korgel, B. A. Supercritical Fluid–Liquid–Solid (SFLS) Synthesis of Si and Ge Nanowires Seeded by Colloidal Metal Nanocrystals. *Adv. Mater.* **2003**, *15*, 437–440.
31. Holmes, J. D.; Johnston, K. P.; Doty, R. C.; Korgel, B. A. Control of Thickness and Orientation of Solution-Grown Silicon Nanowires. *Science* **2000**, *287*, 1471–1473.
32. Heitsch, A. T.; Akhavan, V. A.; Korgel, B. A. Rapid SFLS Synthesis of Si Nanowires Using Trisilane with *in Situ* Alkyl-Amine Passivation. *Chem. Mater.* **2011**, *23*, 2697–2699.
33. Heitsch, A. T.; Fanfair, D. D.; Tuan, H.-Y.; Korgel, B. A. Solution–Liquid–Solid (SLS) Growth of Silicon Nanowires. *J. Am. Chem. Soc.* **2008**, *130*, 5436–5437.
34. Li, J.; Smith, A.; Sanderson, R. J.; Hatchard, T. D.; Dunlap, R. A.; Dahn, J. R. *In Situ*¹¹⁹Sn Mössbauer Effect Study of the Reaction of Lithium with Si Using a Sn Probe. *J. Electrochem. Soc.* **2009**, *156*, A283–A288.
35. Zhou, M.; Pu, F.; Wang, Z.; Cai, T.; Chen, H.; Zhang, H.; Guan, S. Facile Synthesis of Novel Si Nanoparticles–Graphene Composites as High-Performance Anode Materials for Li-ion Batteries. *Phys. Chem. Chem. Phys.* **2013**, *15*, 11394–11401.
36. Zhou, M.; Cai, T.; Pu, F.; Chen, H.; Wang, Z.; Zhang, H.; Guan, S. Graphene/Carbon-Coated Si Nanoparticle Hybrids as High-Performance Anode Materials for Li-Ion Batteries. *ACS Appl. Mater. Interfaces* **2013**, *5*, 3449–3455.
37. Xue, L.; Xu, G.; Li, Y.; Li, S.; Fu, K.; Shi, Q.; Zhang, X. Carbon-Coated Si Nanoparticles Dispersed in Carbon Nanotube Networks as Anode Material for Lithium-Ion Batteries. *ACS Appl. Mater. Interfaces* **2013**, *5*, 21–25.
38. Ng, S. H.; Wang, J.; Wexler, D.; Chew, S. Y.; Liu, H. K. Amorphous Carbon-Coated Silicon Nanocomposites: A Low-Temperature Synthesis via Spray Pyrolysis and Their Application as High-Capacity Anodes for Lithium-Ion Batteries. *J. Phys. Chem. C* **2007**, *111*, 11131–11138.
39. Luo, J.; Zhao, X.; Wu, J.; Jang, H. D.; Kung, H. H.; Huang, J. Crumpled Graphene-Encapsulated Si Nanoparticles for Lithium Ion Battery Anodes. *J. Phys. Chem. Lett.* **2012**, *3*, 1824–1829.
40. Chen, H.; Dong, Z.; Fu, Y.; Yang, Y. Silicon Nanowires with and without Carbon Coating as Anode Materials for Lithium-ion Batteries. *J. Solid State Electrochem.* **2010**, *14*, 1829–1834.
41. Du, C.; Chen, M.; Wang, L.; Yin, G. Covalently-Functionalizing Synthesis of Si@C Core–shell Nanocomposites as High-capacity Anode Materials for Lithium-Ion Batteries. *J. Mater. Chem.* **2011**, *21*, 15692–15697.
42. Yang, Y.; Ren, J.-G.; Wang, X.; Chui, Y.-S.; Wu, Q.-H.; Chen, X.; Zhang, W. Graphene Encapsulated and SiC Reinforced Silicon Nanowires as an Anode Material for Lithium Ion Batteries. *Nanoscale* **2013**, *5*, 8689–8694.
43. Zang, J.-L.; Zhao, Y.-P. Silicon Nanowire Reinforced by Single-Walled Carbon Nanotube and Its Applications to Anti-pulverization Electrode in Lithium Ion Battery. *Composites, Part B* **2012**, *43*, 76–82.
44. Liu, N.; Wu, H.; McDowell, M. T.; Yao, Y.; Wang, C.; Cui, Y. A Yolk-Shell Design for Stabilized and Scalable Li-Ion Battery Alloy Anodes. *Nano Lett.* **2012**, *12*, 3315–3321.

45. Wu, H.; Zheng, G.; Liu, N.; Carney, T. J.; Yang, Y.; Cui, Y. Engineering Empty Space between Si Nanoparticles for Lithium-Ion Battery Anodes. *Nano Lett.* **2012**, *12*, 904–909.
46. Bogart, T. D.; Lu, X.; Korgel, B. A. Precision Synthesis of Silicon Nanowires with Crystalline Core and Amorphous Shell. *Dalton Trans.* **2013**, *42*, 12675–12680.
47. Rathi, S. J.; Jariwala, B. N.; Beach, J. D.; Stradins, P.; Taylor, P. C.; Weng, X.; Ke, Y.; Redwing, J. M.; Agarwal, S.; Collins, R. T. Tin-Catalyzed Plasma-Assisted Growth of Silicon Nanowires. *J. Phys. Chem. C* **2011**, *115*, 3833–3839.
48. Yu, L.; Fortuna, F.; O'Donnell, B.; Patriache, G.; Cabarrocas, P. R. i. Stability and Evolution of Low-Surface-Tension Metal Catalyzed Growth of Silicon Nanowires. *Appl. Phys. Lett.* **2011**, *98*, 123113.
49. Mullane, E.; Kennedy, T.; Geaney, H.; Dickinson, C.; Ryan, K. M. Synthesis of Tin Catalyzed Silicon and Germanium Nanowires in a Solvent–Vapor System and Optimization of the Seed/Nanowire Interface for Dual Lithium Cycling. *Chem. Mater.* **2013**, *25*, 1816–1822.
50. Lee, D. C.; Hanrath, T.; Korgel, B. A. The Role of Precursor-Decomposition Kinetics in Silicon-Nanowire Synthesis in Organic Solvents. *Angew. Chem. Int'l. Ed.* **2005**, *44*, 3573–3577.
51. Holmberg, V. C.; Bogart, T. D.; Chockla, A. M.; Hessel, C. M.; Korgel, B. A. Optical Properties of Silicon and Germanium Nanowire Fabric. *J. Phys. Chem. C* **2012**, *116*, 22486–22491.
52. Chockla, A. M.; Korgel, B. A. Seeded Germanium Nanowire Synthesis in Solution. *J. Mater. Chem.* **2009**, *19*, 996–1001.
53. Olesinski, R. W.; Abbaschian, G. J. The Si–Sn (Silicon–Tin) System. *Bull. Alloy Phase Diagrams* **1984**, *5*, 273–276.
54. Noh, M.; Kwon, Y.; Lee, H.; Cho, J.; Kim, Y.; Kim, M. G. Amorphous Carbon-Coated Tin Anode Material for Lithium Secondary Battery. *Chem. Mater.* **2005**, *17*, 1926–1929.
55. Courtney, I. A.; Tse, J. S.; Mao, O.; Hafner, J.; Dahn, J. R. Ab Initio Calculation of the Lithium-Tin Voltage Profile. *Phys. Rev. B* **1998**, *58*, 15583–15588.
56. Todd, A. D. W.; Ferguson, P. P.; Fleischauer, M. D.; Dahn, J. R. Tin-Based Materials as Negative Electrodes for Li-ion Batteries: Combinatorial Approaches and Mechanical Methods. *Intl. J. Energy Res.* **2010**, *34*, 535–555.
57. McDowell, M. T.; Lee, S. W.; Harris, J. T.; Korgel, B. A.; Wang, C.; Nix, W. D.; Cui, Y. *In Situ* TEM of Two-Phase Lithiation of Amorphous Silicon Nanospheres. *Nano Lett.* **2013**, *13*, 758–764.
58. Liu, X. H.; Zhang, L. Q.; Zhong, L.; Liu, Y.; Zheng, H.; Wang, J. W.; Cho, J.-H.; Dayeh, S. A.; Picraux, S. T.; Sullivan, J. P.; et al. Ultrafast Electrochemical Lithiation of Individual Si Nanowire Anodes. *Nano Lett.* **2011**, *11*, 2251–2258.
59. Liu, X. H.; Fan, F.; Yang, H.; Zhang, S.; Huang, J. Y.; Zhu, T. Self-Limiting Lithiation in Silicon Nanowires. *ACS Nano* **2013**, *7*, 1495–1503.